Block Copolymer Mimetic Self-Assembly of Inorganic Nanoparticles

Yunyong Guo, Saman Harirchian-Saei, Celly M. S. Izumi, and Matthew G. Moffitt*

Department of Chemistry, University of Victoria, P.O. Box 3065, Victoria, BC V8W 3V6, Canada

ABSTRACT Emerging strategies for assembling inorganic nanoparticles into ensembles with multiscale organization are establishing a new paradigm for the synthesis of devices and functional materials with applications ranging from drug delivery to photonics. In this work, the solution self-assembly of amphiphilic ionic block copolymers into morphologically tunable aggregates provides the inspiration and design strategy for nanoparticle building blocks with the essential chemical and conformational features of ionic block copolymer chains in aqueous media. We produce inorganic nanoparticles with surface-tethered mixed brushes of hydrophobic and chargeable hydrophilic chains which self-assemble in polar solvent mixtures into unprecedented hierarchical superstructures analogous to known ionic block copolymer aggregates but with complex organizations of nanoparticles in three dimensions. Electrostatic repulsion between hydrophilic chains forces nonequilibrium pathways to variable kinetic structures with internal lamellar organization of nanoparticles; however, decreasing electrostatic interactions through salt or acid addition allows tunable equilibrium assemblies, including supermicelles and bilayer vesicles of nanoparticles, to be formed. The application of ionic block copolymer assembly principles and mechanisms opens a new chemical toolbox for the organization of nanoparticles into functional assemblies.

KEYWORDS: Inorganic nanoparticles · self-assembly · block copolymers · nanostructured assemblies · structural hierarchy · molecular mimics

The self-assembly of amphiphilic molecular building blocks such as phospholipids and block copolymers provides spontaneous routes to complex function through hierarchical organization, in systems ranging from living cells to modern polymeric materials. In recent years, intriguing opportunities for a new generation of materials and devices have emerged through the potential for combining the optical, electronic, and magnetic properties of colloidal inorganic nanoparticles with the exquisite capacity of molecular amphiphiles for complex three-dimensional (3D) organization.[1−3] Extensive theoretical work has shown that colloidal nanoparticles with surface functionality described by spatially separated and chemically distinct regions ("patchy" or "Janus" particles) will undergo spontaneous self-assembly into complex three-dimensional ensembles *via* anisotropic interparticle interactions, analogous to the ordering of molecular amphiphiles.[4−9]

Specific inspiration for the design and synthesis of colloidal "supermolecules" is provided by amphiphilic block copolymers,[10,11] which undergo solution self-assembly into a diverse range of complex nanostructures, with morphological control provided by experimental variables such as copolymer composition,[12] architecture,[13] polymer concentration,[14] and solvent composition.[15] Two essential features of block copolymer chains are critical to their self-assembly behavior in selective solvents: (1) strong incompatibility between connected and spatially separated chemical sections and (2) conformational flexibility. In recent years, several groups have used these features to establish design principles for the synthesis of amphiphilic nanoparticle building blocks, following a general approach of tethering colloid surfaces with one or more types of polymer chains, enabling nanoparticle self-assembly into several intriguing structures.[16−21]

One such approach involves partially functionalizing nanoparticle surfaces with either hydrophobic or hydrophilic polymer chains, with the unfunctionalized surface regions providing the incompatible chemical section for the resulting amphiphiles. For example, Kumacheva and co-workers selectively functionalized the ends of hydrophilic (cetyl trimethylammonium bromide, CTAB-coated) gold nanorods with hydrophobic polystyrene (PS) brushes to produce amphiphilic "pom-pom" building blocks that spontaneously assembled into rings, chains, bundles, and spheres under different solvent conditions.[17] Subsequently, Förster and co-workers showed that hydrophobic (trioctylphosphine oxide, TOPO-coated) cadmium selenide/cadmium sulfide (CdSe/CdS) core−shell nanoparticles functionalized with hydrophilic polyethylene oxide (PEO) chains formed various solution assemblies, including micelles and vesicles, as the surface density of PEO was varied; in this case, amphiphilic self-assembly was triggered by surface reorganization of PEO chains, leading to anisotropic interparticle attraction between TOPO-coated

* Address correspondence to mmoffitt@uvic.ca.

Received for review February 2, 2011 and accepted March 8, 2011.

Published online March 09, 2011
10.1021/nn200450c

surfaces.[19] A common feature of the nanoparticle amphiphiles described in refs 17 and 19 is that, unlike true block copolymers, only one of the chemical sections is polymeric; the comparable rigidity of the other section may limit the internal complexity of assemblies due to packing constraints, possibly explaining why bilayer or multicompartment nanostructures were not generated in either of those studies.

Closer block copolymer analogues can be produced by functionalizing inorganic nanoparticles with mixed brushes of hydrophilic and hydrophobic chains, such that both of the incompatible chemical sections exhibit conformational flexibility.[16,21] Recently, Li and coworkers described the formation and assembly of gold nanoparticles decorated with bicompartmental brushes of poly(methyl methacrylate) (PMMA) and PEO chains.[21] Incubating the resulting Janus nanoparticles in dioxane resulted in the formation and growth of long, irregular aggregates over time. Zhubarev *et al.* achieved more regular and controllable ensembles of gold nanoparticles by functionalizing the colloid surfaces with V-shaped ligands possessing both PS and PEO arms and investigating their self-assembly in water.[16] It was proposed that the incompatible PS and PEO arms underwent local spatial separation upon water addition to form a Janus structure, followed by amphiphilicity-driven self-assembly into cylinders and vesicles, depending on the initial nanoparticle concentration.

Considering examples of ionic block copolymer self-assembly,[10,12,22−30] we reasoned that greater control, complexity, and diversity should be achievable for amphiphilic organization of mixed brush nanoparticles if one of the polymer chain types was ionic in nature. Along with the chemical variables for morphological control exhibited by nonionic macromolecular amphiphiles, block copolymers containing ionic or ionizable blocks (ionic block copolymers) are additionally tunable *via* changes in pH or ionic strength,[23,24,26] with the potential for increased structural complexity through the free energy contributions of electrostatic interactions.[10,12,25,27−30] Compared to their nonionic counterparts, the extreme incompatibilities between blocks give rise to stronger thermodynamic driving forces for self-assembly in selective solvents, along with higher interfacial tension values leading to sharper interfaces between polymer domains.[22] As well, high interfacial tensions and generally high glass transition temperatures often lead to ionic block copolymer aggregates with extreme kinetic stability,[22] allowing interesting nonequilibrium structures to be trapped.[10,12,29] It is noteworthy that the seminal studies on morphological diversity in block copolymer solutions from the Eisenberg group concerned systems with ionizable poly(acrylic acid) (PAA) blocks.[10,12,22−24] In addition, ionic block copolymers continue to play a dominant role in the development of improved

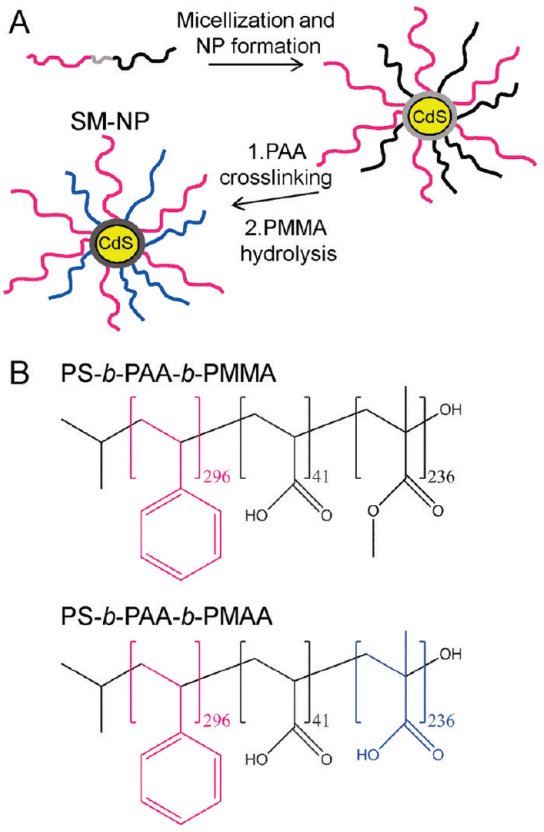

Figure 1. (A) Preparation of SM-NP building blocks and (B) molecular structures of the constituent PS-*b*-PAA-*b*-PMMA triblock copolymer and its hydrolyzed form, PS-*b*-PAA-*b*-PMAA.

control[26] and increased structural complexity[25,27−30] in self-assembling polymeric materials.

In this paper, we describe the synthesis and solution self-assembly of cadmium sulfide (CdS) nanoparticles decorated with mixed brushes of tethered hydrophobic and ionizable hydrophilic (polyacid) polymer chains. The resulting interplay of chain stretching, interfacial tension, and electrostatic interactions harnesses the main elements of ionic block copolymer micellization[22] to enable complex and variable 3D ordering of inorganic nanoparticles in solution without the use of templates. The multiple nanoparticle ensembles that are generated are analogues of several known ionic block copolymer micellar structures, but with complex hierarchical organizations of nanoparticles, including intriguing wormlike colloids with internal nanoparticle lamellae and bilayer vesicles with concentric layers of close-packed nanoparticles. We show that nanoparticle self-assembly pathways can be chemically tuned by adjusting the strength of interchain electrostatic repulsion *via* salt or acid addition. Compared to previous amphiphilic nanoparticles, the combination of extremely strong interfacial tension and interchain electrostatic repulsion afforded by the ionizable chains appears to offer an unprecedented level of control and structural complexity for

nanoparticle self-assembly. Our approach opens a new chemical toolbox for producing functional nanoparticle ensembles, while bridging concepts in molecular self-assembly with the realm of colloidal nano-objects.

RESULTS AND DISCUSSION

We apply a self-assembly strategy to forming block copolymer mimetic polymer/inorganic hybrid nanoparticles (Figure 1A). This approach starts with micellization of a polystyrene-*block*-poly(acrylic acid)-*block*-poly(methyl methacrylate) (PS-*b*-PAA-*b*-PMAA) triblock copolymer (Table 1, Figure 1B) *via* assembly of ionized cadmium (Cd^{2+})-complexed PAA blocks in organic solvent. Next, reaction with hydrogen sulfide (H_2S) produces CdS nanoparticles surrounded by a solubilized mixed-brush layer of statistically distributed PS and PMMA chains, as described in our previous paper.[31] Finally, we render the nanoparticles amphiphilic by cross-linking the PAA layer at the CdS-polymer interface with a combination of cadmium acetate and diamide-forming 2,2′-(ethylenedioxy)diethylamine (EDDA), followed by base-catalyzed hydrolysis of PMMA blocks to poly(methacrylic acid) (PMAA) (Figure 1B).

TABLE 1. Characteristics of PS-*b*-PAA-*b*-PMMA Triblock Copolymer

M_n, g/mol	M_w/M_n	N_{PS}[a]	N_{PAA}	N_{PMMA}
59700	1.05	296	41	236

[a] Number-average degrees of polymerization of the respective blocks, determined as described in ref 31.

The resulting core-cross-linked micelles (designated SM-NPs) consist of a CdS nanoparticle surrounded by a tethered mixed brush of hydrophobic PS and hydrophilic PMAA chains with an estimated surface density of ~0.8 chain/nm^2.[31] SM-NPs can be dispersed without aggregation to form clear dispersions in polar organic solvents such as tetrahydrofuran (THF) and dimethylformamide (DMF) (see dynamic light scatting (DLS) results in Figure S3). Transmission electron microscopy (TEM) images of individual SM-NPs deposited from THF solution (Figure 2A) show well-separated dark dots attributed to CdS nanoparticles in the cores (diameter =5.8 ± 0.4 nm). The inset is a high resolution TEM (HRTEM) image of a single CdS nanoparticle showing clear lattice lines; X-ray diffraction (XRD) indicates a cubic crystalline CdS structure for both SM-NPs and their various assemblies (Figure S4).

The amphiphilicity and stability of SM-NPs make them suitable building blocks for subsequent self-assembly steps, allowing complex structural hierarchy to be built up within nanoparticle ensembles. Dropwise water addition to SM-NPs dissolved in THF triggers a sudden increase in turbidity, indicating self-assembly into secondary structures. Figure 2B shows TEM images of the resulting suspension following transfer into a pure water environment, revealing spherical assemblies with a mean diameter of ~140 nm containing multiple CdS nanoparticles (dark dots). TEM of thin ultramicrotomed sections (Figure 2B, inset) shows that the CdS nanoparticles are localized at the surfaces of PS (gray) spheres; reverse-contrast images from high-angle annular dark field (HAADF) TEM

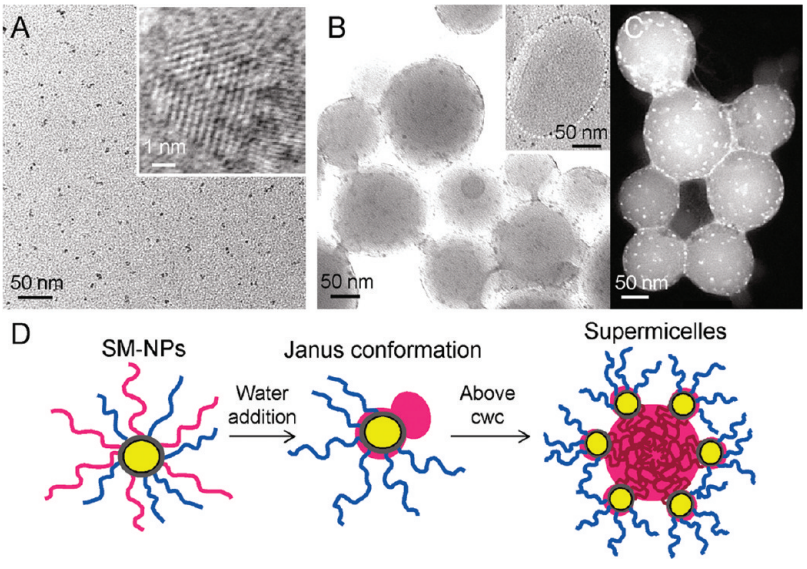

Figure 2. (A) TEM image of individual SM-NPs and HRTEM image (A, inset) of a single SM-NP crystalline CdS nanoparticle core showing electron diffraction lines. (B) TEM image of secondary spherical assemblies produced by adding 75 wt % water dropwise to 0.5 wt % SM-NPs in THF (cwc ~12 wt % water), followed by immediate transfer into excess water; TEM of a microtomed section shows CdS nanoparticles (dark dots) localized at the PS core surface of a supermicelle (B, inset). (C) HAADF image of supermicelles in which CdS nanoparticles appear as bright dots. (D) Mechanism of amphiphilic SM-NP assembly: water addition induces intraparticle spatial separation of PS and PMAA chains (Janus conformation), followed by interparticle aggregation of PS sections and supermicelle formation above the critical water content (cwc).

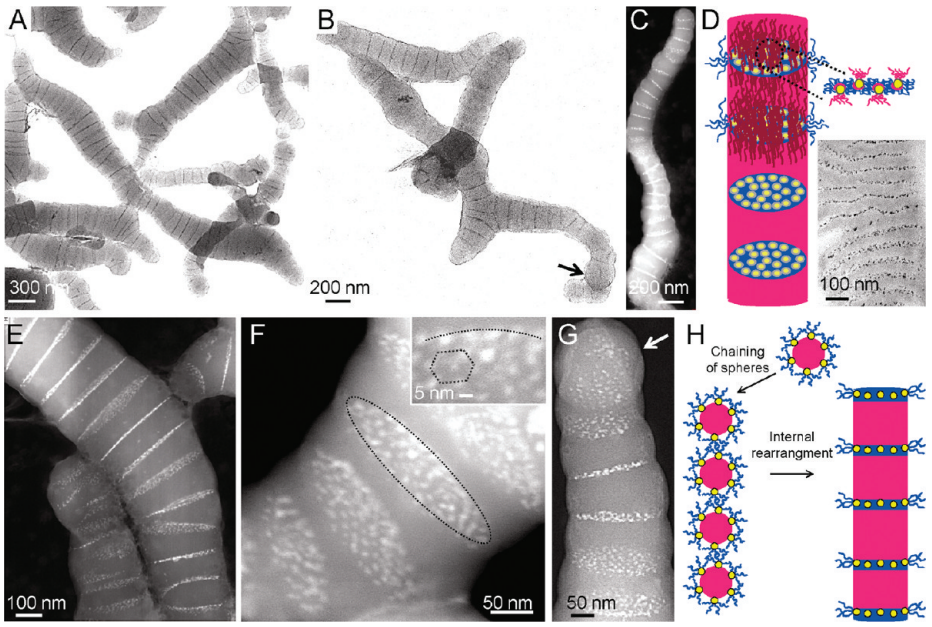

Figure 3. Tertiary wormlike assemblies produced by adding 75 wt % water dropwise to 1.0 wt % SM-NPs in THF (cwc ~10 wt % water), followed by immediate transfer into excess water. (A and B) TEM and (C) HAADF images showing the segmented structure of the assemblies. (D) Schematic of lamellar ordering of SM-NPs; TEM image of a microtomed section of a wormlike assembly (D, inset) indicates internal alternating layers of PS (gray) and CdS nanoparticles (dark dots) dispersed within PMAA (light). (E, F, and G) HAADF images highlighting regularly spaced disks containing two-dimensional arrays of CdS nanoparticles (bright dots) with preferred hexagonal ordering (F, inset). (H) Mechanism of wormlike assembly formation: secondary spherical supermicelles form tertiary one-dimensional aggregates, followed by internal rearrangement of spheres into cylindrical segments. Arrows in B and G indicate spheres that did not convert into segments before kinetic freezing.

(Figure 2C) allow a surface density of ~1000 nanoparticles (light dots)/μm^2 to be determined.[32]

The structure of the spherical aggregates points to a mechanism of amphiphilic self-assembly of SM-NPs (Figure 2D): as water is added dropwise to THF, individual SM-NPs first rearrange into a Janus structure by intraparticle spatial separation of PS and PMAA *via* wrapping of chains around the core; in this conformation, SM-NPs resemble block copolymer amphiphiles with a CdS nanoparticle at the hydrophobic/hydrophilic junction. With continued water addition, a critical water content (cwc) is eventually reached at which hydrophobic interactions between PS sections trigger SM-NP assembly into supermicelles with a PS core, PMAA corona, and CdS nanoparticles localized at the PS/PMAA interface. The term "supermicelle" is applied in reference to the higher-order organization of primary micellar building blocks; we note that the word has been similarly used by Eisenberg and co-workers to describe a different type of colloidal assembly of triblock copolymers and CdS nanoparticles.[33] Compared to simple spherical micelles of block copolymer chains,[12] the high size polydispersity and large degree of PS stretching indicated by the mean core diameter[34] suggest that SM-NP supermicelles formed under these conditions are nonequilibrium structures.

By increasing the initial SM-NP concentration by a factor of 2, the same method of water addition described above generates the interesting wormlike structures shown in Figure 3. Figure 3A and B show linear and Y-shaped cylindrical aggregates up to several micrometers in length with a segmented structure of periodic gray bands and darker lines. The regular spacing of high electron density lines is distinctly observed in the reverse contrast HAADF image of an individual aggregate (Figure 3C). From TEM of ultramicrotomed sections (Figure 3D, inset), the internal structure of wormlike assemblies consists of lamellae of alternating PS (gray) and PMAA (light) layers, with CdS nanoparticles (dark dots) localized within the PMAA. Due to the cylindrical shape of the segments, the thin PMAA/CdS nanoparticle layers are disk-shaped (Figure 3E and F); a close-up view of several disks with normal axes slightly rotated out of the image plane (Figure 3F) highlights the hierarchical organization of CdS nanoparticles. Within each disk, CdS nanoparticles are arranged in a single plane with several groupings indicating preferred hexagonal packing and an estimated interparticle spacing of ~10 nm (Figure 3F, inset); the mean spacing between disks is 106 nm and remarkably uniform (relative standard deviation = 6%). The internal organization of wormlike assemblies (Figure 3D) is the product of lamellar ordering of Janus-arranged SM-NPs aligned along the cylinder long axis; we speculate that some PMAA chains attached to SM-NPs situated at the disk edges form a solubilized coronal layer, preventing colloid agglomeration in water.

These wormlike nanostructures bear a striking visual resemblance to annelids, although a more significant

parallel to living systems is their high degree of structural hierarchy, achieved *via* a series of multiple self-assembly steps involving increasingly complex building blocks. The spontaneous formation of wormlike aggregates from SM-NPs is explained by a two-step assembly process induced by water addition. Above the cwc, PS sections of Janus-arranged SM-NPs first aggregate to form secondary spherical supermicelles, similar to those formed at lower initial SM-NP concentration. However, the higher particle concentration allows a subsequent one-dimensional tertiary assembly of spheres to occur, followed by rearrangement of the spheres into cylindrical segments, prior to kinetic freezing at high water contents (Figure 3H). The formation of branch points leading to Y-shaped aggregates is the kinetic product of spherical supermicelle polydispersity and is, thus, more closely related to branching in kinetically controlled block copolymer cylinders[29] than to equilibrium Y-junctions associated with internal curvature optimization.[35] Visual evidence for the proposed two-step mechanism comes from wormlike assemblies with spheres at an end (Figure 3G) or along their length (Figure 3B) that did not have time to evolve into cylindrical segments.

The driving force for one-dimensional assembly of spherical supermicelles is provided by partial dissociation of methacrylic acid groups as water is added, which gives rise to increasing electrostatic repulsion between partially charged and densely grafted PMAA chains on each SM-NP subunit. Even at water concentrations just above the cwc, the PMAA sections of Janus-arranged SM-NPs will be partially ionized due to the preferential distribution of water around locally concentrated PMAA segments,[24] with ionization increasing as the water content rises. Covalent cross-linking within the SM-NP cores precludes a lowering in PMAA packing density in response to the increasing electrostatic repulsion; solubilized chains therefore become progressively stretched until the resulting entropic penalty triggers the solution phase separation of PMAA *via* aggregation of spherical supermicelles. An additional driving force for tertiary assembly may be supplied by electrostatic attraction between PMAA chains and CdS surfaces of approaching spheres, as evidenced by the strong interpenetration of CdS nanoparticles and PMAA within the internal lamellae. We note the structural and mechanistic similarities of SM-NP assembly into wormlike nanostructures with recently described hierarchically ordered block copolymer aggregates formed under kinetic control;[29] this underlines the potential of exploiting complex assembly modes using nanoparticles engineered to mimic chemical and conformational features of block copolymer chains.

Although the internal lamellar structure represents a local free energy minimum for SM-NPs in THF/water mixtures, the one-dimensional assembly process

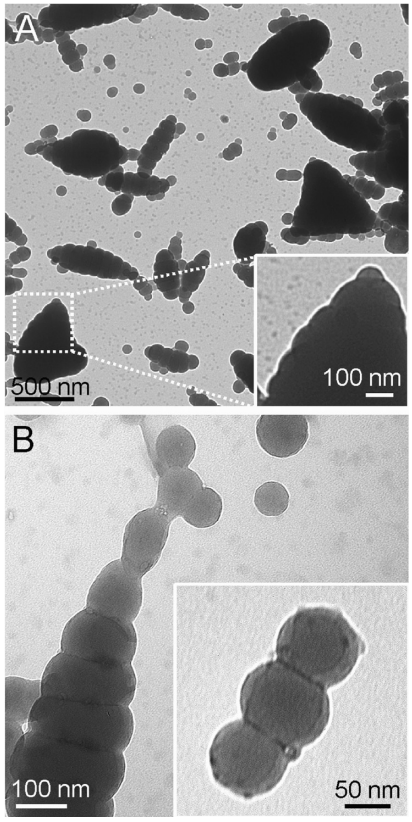

Figure 4. Various assemblies produced by adding 11 wt % water to 1.0 wt % SM-NPs in THF followed by two weeks of annealing. (A) TEM image showing several triangular and elliptical aggregates, with a segmented structure similar to wormlike assemblies, indicating internal lamellar ordering of nanoparticles. The segmented structure of one of the triangular aggregates is more clearly shown in the higher magnification image in the inset. (B) TEM images highlighting the coexistence of spheres and short chains of spheres under these conditions.

described above is kinetically controlled, with the wormlike morphology (Figure 3) being trapped by immediate transfer into an aqueous environment in which slow chain dynamics preclude further progress to global equilibrium. This is demonstrated by dramatic changes in morphology when nanoparticle assemblies are annealed at various water contents for two weeks prior to kinetic freezing; under these conditions, assembly shapes are influenced by a combination of fast one-dimensional assembly and subsequent slow growth of the low energy lamellae. For example, annealing in THF/11 wt % water (Figure 4A and B), just above the cwc, gives rise to a coexistence of small spheres and short chains of spheres, presumably formed immediately upon water addition above the critical concentration. Additional segmented ellipsoidal and triangular aggregates (Figure 4A) are explained by the slower growth of lamellae along the short axes of linear and branched tertiary aggregates over the long annealing period. The presence of secondary spheres and the relatively short lengths of the one-dimensional assemblies (Figure 4B) suggest a low

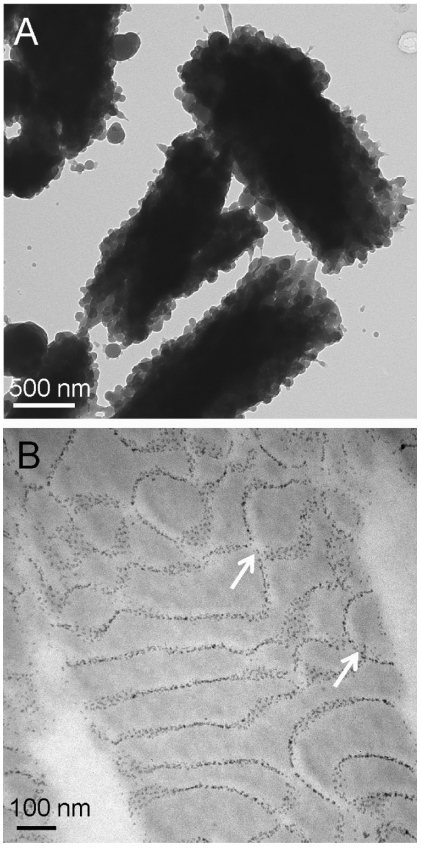

Figure 5. Rectangular assemblies produced by adding higher water contents to 1.0 wt % SM-NPs in THF followed by two weeks of annealing. (A) TEM image of rectangular aggregates formed at 25 wt % water in THF. (B) Microtomed section of a rectangular aggregate formed at 50 wt % water in THF, showing internal lamellar ordering of nanoparticles; circular and curved transition structures (arrows) suggest growth of lamellae *via* addition of spherical supermicelles.

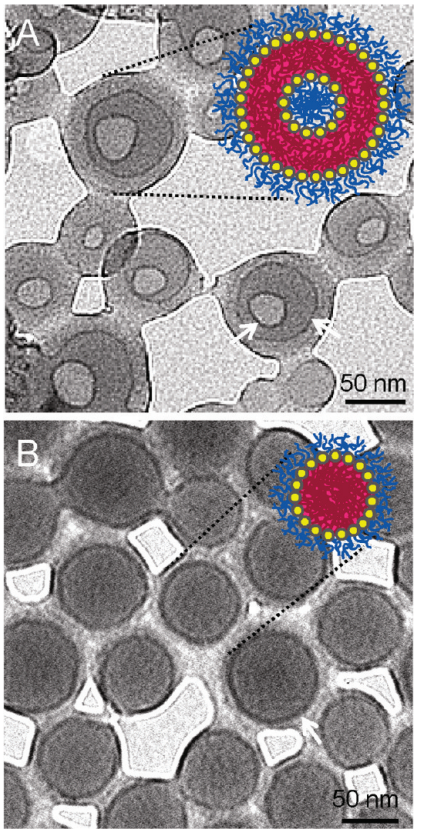

Figure 6. Equilibrium assemblies produced by adding 75 wt % water dropwise to SM-NPs in THF containing small quantities of NaCl. (A) TEM images of vesicles (1.0 wt % SM-NPs, R_{NaCl} = 3.0) consisting of a bilayer arrangement of SM-NPs (inset) forming two concentric shells of densely packed CdS nanoparticles (indicated with arrows). (B) TEM image of equilibrium supermicelles (0.5 wt % SM-NPs, R_{NaCl} = 1.5) consisting of a spherical arrangement of SM-NPs (inset) forming a shell of densely packed CdS nanoparticles on the PS core surface (indicated with an arrow).

driving force for tertiary assembly formation at 11 wt % water, compared to the formation of wormlike assemblies when water is added continuously up to 75 wt %.

For annealing at higher water contents, THF/25 wt % (Figure 5A) and THF/50 wt % water (Figure 5B), a similar combination of fast one-dimensional assembly and slow lamellar growth gives rise to sheet-like rectangular assemblies. A microtomed section in the plane of a rectangular aggregate (Figure 5B) reveals an internal organization of lamellae with a preferred orientation perpendicular to the long axis; the circular and curved nanoparticle organizations represent transition structures from spherical supermicelles added during one-dimensional aggregation or subsequent growth and trapped in the process of incorporating into existing lamellae.

By chemically attenuating electrostatic interactions of PMAA, which drive the formation and growth of the various kinetically controlled aggregates described above, equilibrium pathways to completely different nanoparticle ensembles can be triggered. Specifically, the addition of salt serves to screen electrostatic repulsion between partially ionized methacrylic acid groups, thus stabilizing solution solubilization of PMAA. This activates assembly processes analogous to equilibrium formation of block copolymer micelles, in which the resulting nanostructures are a thermodynamic balance of core chain stretching, coronal chain repulsion, and core/corona interfacial tension.

For example, relatively uniform spheres with central cores of higher electron transmission, consistent with bilayer vesicles of SM-NPs (Figure 6A), are formed under conditions identical to wormlike nanostructure formation, except for the presence of a small quantity of NaCl added as an aqueous solution prior to dropwise water addition (molar ratio of NaCl to methacrylic acid repeat units, R_{NaCl} = 3.0). The vesicles constitute an interesting organization of SM-NPs in which PMAA chains are solubilized within encapsulated water pools and in external coronae, a bilayer of insoluble PS chains make up the vesicle walls, and amphiphile junctions form two concentric monolayers of densely packed CdS nanoparticles at low curvature PS/PMAA interfaces. The extremely uniform spacing between close-packed CdS nanoparticle layers within the vesicles is 24 $\pm$ 4 nm, as determined by the PS wall thickness. Almost identical

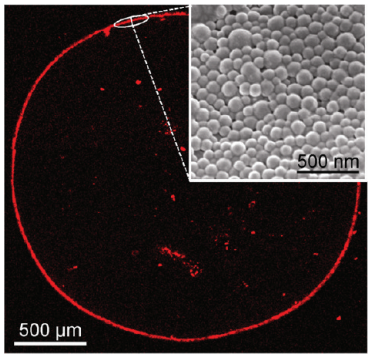

Figure 7. LSCFM image of "coffee ring" pattern of photoluminescent vesicles (composite image of four micrographs of each ring quadrant) produced by evaporative assembly of SM-NP vesicles on a glass substrate. The inset shows an accompanying SEM image of the assembled vesicles.

vesicle structures are also obtained by replacing NaCl with HCl, which protonates methacrylic acid groups to minimize electrostatic repulsion (Figure S10). The photoluminescence of the SM-NP vesicles is demonstrated by CdS light emission from an assembled "coffee-ring" pattern of close-packed vesicles formed by evaporative deposition on a glass substrate, as shown by the laser scanning confocal fluorescence microscopy (LSCFM) image (Figure 7) and accompanying scanning electron micrograph (SEM) (Figure 7, inset).

The capabilities of transport and compartmentalization provided by biological and synthetic bilayer membranes, including vesicles, have found applications ranging from cosmetics to the controlled delivery of anticancer agents.[11,36,37] The self-assembly of inorganic nanoparticles into bilayer vesicles offers opportunities for colloidal devices in which combinations of magnetic, optical, and electronic function can be integrated with the structural capacity for encapsulation. To our knowledge, this is the first example of nanoparticle self-assembly into bilayer vesicles possessing distinct concentric nanoparticle layers. Förster and co-workers produced interesting monolayer vesicles from amphiphilic gold nanoparticles, although the lack of conformational flexibility of hydrophobic TOPO-coated surfaces precluded their packing into bilayer structures.[19] Vesicle structures produced by Zubarev et al. from mixed brush coated colloidal gold showed nanoparticle localization within the vesicle walls, although without a clear bilayer arrangement, possibly due to the relatively short length (~40 repeat units) of the hydrophobic arms or to insufficient segregation strength between constituent PS and PEO chains.[16]

Similar to salt- and acid-induced morphology transformations in block copolymer micelles,[23,24] we find that the interfacial curvature and thus the morphologies of equilibrium SM-NP assemblies can be tuned by varying the salt or acid content. For instance, decreasing the salt to methacrylic acid ratio to $R_{NaCl} = 1.5$ prior to self-assembly increases electrostatic repulsion within the PMAA corona, which favors the formation of high curvature spherical supermicelles with densely packed CdS nanoparticles at the PS core surface (mean diameter = 69 nm) (Figure 6B); increased core dimensions from 24 to 69 nm indicates increased PS stretching compared to vesicles, consistent with the curvature change.[12] Compared to the spherical supermicelles formed by kinetic control in the absence of added salt (Figure 2B and C), the spheres in Figure 6B are smaller and more uniform with a denser packing of CdS nanoparticle junctions, suggesting that they are equilibrium assemblies of SM-NP units.

CONCLUDING REMARKS

In summary, we demonstrate that inorganic nanoparticles coated with mixed polymer brushes of hydrophobic and partially charged hydrophilic chains undergo amphiphilic self-assembly to form multiple colloidal nanostructures with hierarchical organizations of nanoparticles. Although the promise of complex nanoparticle self-organization based on the principles of block copolymer assembly has been actively pursued in recent years,[1−9,16−21] the structural variability and complexity demonstrated in experimental studies to date[16−21] have fallen short of block copolymers in selective solvents,[10−15,22−30] due to conformational and/or chemical limitations in the amphiphilic colloids that have been produced. We show that by combining conformational flexibility, extremely strong polymer/polymer segregation, and electrostatic interactions in colloidal building blocks, nanoparticle self-assembly with unprecedented complexity and control can be achieved. The ability to produce such spontaneous and hierarchical organizations of nanoparticles provides a versatile colloidal platform for engineering specific collective optical, electronic, and magnetic functionality *via* controlled interactions between nanoparticles with various individual properties. We anticipate that future work on block copolymer mimetic nanoparticle assembly will generate both opportunities and challenges, as new structure−function relations are developed en route to a plethora of exciting device structures for drug delivery, bioimaging, and photonics.

METHODS

Synthesis of Polystyrene-*block*-Poly(acrylic acid)-*block*-Poly(methyl methacrylate) (PS-*b*-PAA-*b*-PMMA) Triblock Copolymer. The polystyrene-*block*-poly(*tert*-butyl acrylate)-*block*-poly(methyl methacrylate) (PS_{296}-*b*-P*t*BA_{41}-*b*-$PMMA_{236}$; subscripts indicate number average degrees of polymerization of the corresponding blocks) triblock copolymer used as a precursor material in the present study was synthesized using anionic polymerization techniques described elsewhere in the literature.[38,39] Following synthesis and characterization of PS_{296}-*b*-P*t*BA_{41}-*b*-$PMMA_{236}$, the middle P*t*BA block was

selectively hydrolyzed to form polystyrene-*b*-poly(acrylic acid)-*b*-poly (methyl methacrylate) (PS_{296}-*b*-PAA_{41}-*b*-$PMMA_{236}$) by reflux in toluene with *p*-toluenesulfonic acid (5 mol % relative to the *tert*-butylacrylate content) for 5 h. Further details on the synthesis and characterization of PS_{296}-*b*-PAA_{41}-*b*-$PMMA_{236}$ (Table 1) can be found in our previous paper.[31]

Synthesis of Amphiphilic SM-NP Nanoparticles. The synthesis of amphiphilic SM-NP nanoparticles begins with identical steps to those followed for the formation of cadmium sulfide nanoparticles with mixed PS/PMMA brush layers (designated PS/PMMA-CdS) described in our previous paper.[31] The reader is also referred to ref 31 for detailed light scattering and 2D NOESY ^{1}H NMR characterization of the structure and polymer brush density of PS/PMMA-CdS nanoparticles, which is assumed to be identical to that of SM-NPs following hydrolysis of PMMA coronal blocks due to covalent cross-linking of the micelle cores. (This assumption was verified by the absence of single chains leaching from the micelles during hydrolysis, as determined by GPC data, Figure S2, as discussed in a subsequent paragraph.)

First, the triblock copolymer PS_{296}-*b*-PAA_{41}-*b*-$PMMA_{236}$ was dissolved in benzene/methanol (90:10 v/v) at a concentration of ca. 2 wt %. The self-assembly of insoluble poly(cadmium acrylate) (PACd) blocks was induced by the addition of excess 0.25 M cadmium acetate dihydrate (Aldrich) in methanol (1.5 mol of cadmium acetate dihydrate/1 of mol acrylic acid repeat units) followed by stirring of the solution for 4 h. The onset of a bluish tinge upon addition of cadmium acetate indicated an increase in light scattering caused by the formation of reverse micelles with PACd cores. The copolymer micelles (kinetically stable due to the high glass transition temperature of the PACd cores) were recovered by freeze-drying and then dried in a vacuum oven at 70 °C for 24 h. Excess cadmium acetate was removed by washing the freeze-dried powder repeatedly with methanol followed by drying under vacuum at 70 °C for 24 h.

The growth of CdS nanoparticles in the Cd^{2+}-containing cores of PS-*b*-PACd-*b*-PMMA micelles was carried out by leaving the micelles in an atmosphere of 100% humidity for 1 week followed by exposure to wet H_2S for a total of 24 h. In order to stabilize the resulting CdS-containing micelles for subsequent hydrolysis and amphiphilic self-assembly, the reprotonated PAA layer at the CdS/copolymer interface was cross-linked with a combination of divalent cadmium ions and covalent diamide groups[40−42] in the following manner: first, the yellow powder was dispersed in THF to 2 wt %, followed by the immediate fast addition of 0.5 equiv of cadmium acetate dihydrate in methanol (0.5 mol of cadmium acetate dehydrate/1 mol of acrylic acid repeat units), and the solution was stirred overnight. Then, a 1.0 wt % solution of *N*-ethyl-*N*′-(3-dimethylaminopropyl)-carbodiimide methiodide (EDC) activator in deionized water was added (0.5 mol of EDC/1 mol of acrylic acid repeat units) all at once, and the solution was left to react for 30 min with stirring. Finally, a 1.0 wt % solution of 2,2′-(ethylenedioxy)bis-(ethylamine) (EDDA) in water was added in one portion (0.25 mol of EDDA/1 mol of acrylic acid repeat units) and the reaction solution was stirred overnight. The sample was recovered by precipitating into methanol, washed repeatedly with methanol, and then dried for 24 h under vacuum at 70 °C. The cross-linked product was designated PS/PMMA-CdS_{XL}.

To hydrolyze the PMMA ester groups, PS/PMMA-CdS_{XL} was dissolved to 10 wt % in 1,4-dioxane with 2 mol of KOH/1 mol of methyl methacrylate repeat units and 18-crown-6 as a phase transfer catalyst (0.2 mol of [18-crown-6]/1 mol of methyl methacrylate repeat units) under argon in a sealed high-pressure Schlenk tube; the reaction was carried out at 110 °C for 4 days. To recover the hydrolyzed product, the solution was further diluted with 1,4-dioxane, precipitated into 0.2 M acetic acid (2 mol of acetic acid/1 mol of methyl methacrylate repeat units), and then dried under vacuum at 60 °C for 24 h. The ^{1}H NMR spectra and peak assignments in Figure S1 confirm essentially complete hydrolysis of PMMA to PMAA in the mixed brush layer. Gel permeation chromatography (GPC) confirmed that no single chains were leached from the core-cross-linked micelles during hydrolysis (Figure S2). The hydrolysis reaction yields the amphiphilic nanoparticles PS/PMAA-CdS_{XL}, which for simplicity are designated SM-NPs to indicate styrene (S) and methacrylic acid (M) repeat units in the external mixed brush and an inorganic nanoparticle (NP) in the core.

Self-Assembly of SM-NPs in Mixtures of THF and Water. Unless otherwise stated, the various nanoparticle assemblies described in this paper were produced using the following general procedure: SM-NPs micelles were dissolved in THF to form ∼2 g solutions with initial SM-NP concentrations 0.5 or 1.0 wt %. The THF used was 99.9+ % HPLC grade ([H_2O] < 0.02 wt %). To each solution, deionized water was added dropwise at a rate of 10 μL/10 s with rapid stirring. During water addition, the point at which a sudden increase in turbidity indicated the onset of SM-NP self-assembly was visually observed and recorded as the critical water concentration (cwc). After the cwc, water addition was continued at the same rate up to 75 wt % water and then the solution was immediately dumped into 10 g of deionized water to kinetically freeze the aggregates. The self-assembled samples were then dialyzed against deionized water for 5 days to remove residual organic solvent. For all experiments, the stirring rate during water addition was held approximately constant by using the same setting on the stir plate with the same stir bars. The room temperature was measured to be 23 ± 1 °C for all self-assembly experiments. Aqueous assembled nanoparticle colloids were sealed with Teflon in vials and stored in a dark drawer when not in use.

Annealed SM-NP assemblies in various mixtures of water and THF were prepared using the following procedure: SM-NPs were dissolved in THF solutions to form ∼2 g solutions, each with an initial SM-NP concentration of 1.0 wt %. To each solution, water was added dropwise at a rate of 10 μL/10 s up to three different water contents above the cwc (11, 25, 50 wt %) with rapid stirring. The four solutions were stirred at medium speed for 2 weeks and then dumped into 10 g of water to kinetically freeze the aggregates. Finally, the solutions were dialyzed against deionized water for 5 days to remove residual THF.

Equilibrium SM-NP assemblies were prepared by allowing SM-NPs to self-assemble in a solvent environment containing salt or strong acid in which electrostatic repulsion between PMAA chains was attenuated. To this end, SM-NPs were dissolved in THF solutions to form ∼2 g solutions with initial SM-NP concentrations of 0.5 or 1.0 wt %. Then, a small quantity of either NaCl or HCl was added as an aqueous solution, with the total water content after NaCl or HCl addition being well below the cwc. For salt addition experiments, the NaCl to methacrylic acid ratios investigated were R_{NaCl} = 1.5 or 3.0, and for the strong acid addition experiment, the HCl to methacrylic acid ratio was R_{HCl} = 0.8. To each solution, deionized water was added dropwise at a rate of 10 μL/10 s with rapid stirring up to 75 wt % water. The solutions were immediately dumped into 10 g of deionized water to kinetically freeze the aggregates, followed by dialysis against deionized water for 5 days to remove residual THF.

Gel Permeation Chromatography (GPC). GPC measurements were performed using a Viscotek Model 302 liquid chromatography system equipped with refractive index (RI), low-angle light scattering (LALS, θ = 7°), right-angle light scattering (RALS, θ = 90°), and UV detectors. THF was used as the eluent at a flow rate of 1 mL/min, and the column temperature was set at 35 °C. All polymer solutions were filtered through membrane filters with a nominal pore size of 0.45 μm before injection into the GPC column. The data were collected and analyzed on a Dell Dimension 2300 computer with appropriate GPC software from Viscotek. Two ViscoGEL HR High-Resolution columns (styrene-divinyl benzene columns) in series were used: G3000 HR 60 k and GMHHR-M Mixed Bed 4 M columns.

^{1}H NMR. ^{1}H NMR spectra were recorded using a Bruker AC 300 MHz spectrometer.

UV−vis Absorption and Photoluminescence Measurements. Absorption spectra were recorded on a Cary 50-scanning UV−vis spectrophotometer. Static photoluminescence (PL) measurements were recorded on an Edinburgh Instruments FLS 920 instrument equipped with a Xe 450 W arc lamp and a red-sensitive PMT (R928-P). For PL measurements, SM-NPs were dispersed in THF at a concentration such that the measured absorbance at 400 nm was less than 0.1. PL measurements

involved λ_{ex} = 400 nm excitation and collection of emitted light with a FEL 500 edge filter in place, scanning from 500 to 790 nm emission at 0.5 nm step size and subtracting a solvent background.

Transmission Electron Microscopy (TEM). Routine TEM imaging was performed on a Hitachi H-700 electron microscope, operating at an electron accelerating voltage of 75 kV. Solution-cast samples of SM-NPs were prepared by depositing a drop of 2 mg/mL solution in THF on a copper grid (300 mesh) coated with an amorphous carbon film with immediate blotting of the excess solution; the grids were then dried at room temperature for 2 h before imaging. For TEM of various SM-NP assemblies in aqueous solutions, the original solutions were diluted to a concentration of 0.5 mg/mL, and then a 10 μL drop was deposited on a carbon/Formvar-coated 300-mesh copper grid with immediate blotting of the excess solution; the grids were then dried at room temperature for 2 h before imaging. Particle size analysis and statistics of various feature dimensions were carried out on the images, with regions of the TEM grids randomly sampled and a minimum of 100 particles measured and included in each analysis.

In order to better observe the internal structure of various aggregates, powdered samples obtained by drying the aqueous solutions were embedded in epoxy resin (Epon), and then ~50 nm-thick sections were obtained with a diamond knife on a Reichert UltraCut E ultramicrotome. The thin sections were then placed on carbon/Formvar-coated 300 mesh copper grids for imaging.

High-resolution TEM imaging was carried out on an FEI Tecnai scanning transmission electron microscope (STEM), operating at an accelerating voltage of 200 kV. This instrument allowed high-angle annular dark-field (HAADF) STEM images to be obtained for improved contrast within various nanoparticle assemblies. Energy-dispersive X-ray spectroscopy (EDX) was performed using an energy-dispersive X-ray detector installed on the FEI Tecnai STEM with an energy resolution of 1.36 eV for Mn Kα radiation; the scan time was 90 s.

Powder X-ray Diffraction (XRD). To prepare the SM-NP sample for XRD, about 15 mg of powdered SM-NPs were dissolved in ethanol and smeared onto a zero-background holder. For XRD experiments on SM-NP assemblies, the various aqueous dispersions, each at a concentration of ~0.5 wt %, were cast directly onto the sample holder and then allowed to evaporate and air-dry. Step-scan X-ray powder diffraction data were obtained over the 2θ range 20°−100° with Cr (30 kv, 15 mA) (wavelength is 0.228 nm) radiation on a Rigaku Miniflex diffractometer with a variable divergence slit, 4.2° scattering slit, and 0.3 mm receiving slit. The scanning step size was 0.02° with a counting time of 6 s per step.

Dynamic Light Scattering (DLS). DLS experiments on SM-NPs in THF and DMF were carried out on a Brookhaven Instruments photocorrelation spectrometer equipped with a BI-200SM goniometer, a BI-900AT digital autocorrelator, and a Melles Griot He−Ne laser (632.8 nm) with a maximum power output of 75 mW. All DLS measurements were conducted at 23 °C.

Atomic Force Microscopy (AFM). A Veeco AFM Instrument equipped with a Veeco tip (Nanoprobe-MLCT-EXMT-A) running in contact mode was used to obtain AFM images of SM-NP assemblies cast from aqueous dispersions onto clean glass microscope coverslips. The effect of vibration was minimized by a vibration-resistant housing on a vibration isolation platform maintained at 80 psi. Each sample was imaged several times at different locations on the substrate. The statistical analysis of heights and full width half-maximum (fwhm) widths of SM-NP assemblies was carried out by measuring surface height profiles for at least 100 features in different regions of suitable AFM images.

Laser Scanning Confocal Fluorescence Microscopy (LSCFM). Laser scanning confocal fluorescence microscopy of SM-NP assemblies cast from aqueous dispersions onto clean glass microscope coverslips was carried out on a Zeiss LSM 410 equipped with an Ar/Kr laser. All films were excited at 488 nm, using a band-pass 485 ± 20 nm line selection filter and an FT 510 dichroic beam splitter; a long-pass 515 nm emission filter was employed such that only light above 515 nm reached the PMT. For LSCFM of wormlike assemblies, a Zeiss Plane-Aprochromat 63× oil-immersion objective was used for imaging with a pinhole diameter of 1.31 Airy units, resulting in an optical section thickness of 0.75 μm fwhm. For LSCFM of the "coffee ring" of vesicle assemblies, a Zeiss 10× objective lens was used for imaging with a pinhole diameter of 3.4 Airy units. For each sample containing CdS nanoparticles, a suitable control sample without CdS nanoparticles was run to confirm that contrast was from CdS photoluminescence and not from the scattering of excitation light.

Zeta Potential Measurement. Zeta potentials and hydrodynamic particle sizes of various SM-NP assemblies in water were measured at different pH values using a Zeta PALS Analyzer (Brookhaven Instruments Corporation, USA). Zeta potential values were calculated from electrophoretic mobility values using the Smoluchowski equation. The hydrodynamic size analysis of the samples was conducted by photon correlation spectroscopy (PCS) measurements through a BI-9000 Brookhaven light scattering apparatus (Brookhaven Instrument Cooperation), fitted with a 20 mW He−Ne laser, with the detector angle set at 90°. The various aqueous colloids were diluted with a 0.01 M NaCl aqueous solution to a concentration of about 0.05 mg/mL NaCl as a salt background. The pH values of the aqueous solutions were adjusted by titrating 0.1 M HCl and NaOH solutions. The zeta potential and size analysis was carried out at 25 °C.

Acknowledgment. We thank the Natural Science and Engineering Council (NSERC) of Canada, the Canadian Foundation for Innovation (CFI), and the British Columbia Knowledge Development Fund (BCKDF) for their support of this work. C. M.S.I. is grateful for the support of CAPES (Brazil). We also thank Profs. Mitchell A. Winnik and Eugenia Kumacheva for helpful comments. The authors would like to dedicate this paper to Prof. A. Eisenberg, in honor of his distinguished and inspiring scientific career.

Supporting Information Available: Experimental details and images. This material is available free of charge via the Internet at http://pubs.acs.org.

REFERENCES AND NOTES

1. Glotzer, S. C.; Solomon, M. J. Anisotropy of Building Blocks and their Assembly into Complex Structures. *Nat. Mater.* **2007,** *6*, 557–562.
2. Nie, Z.; Petukhova, A.; Kumacheva, E. Properties and Emerging Applications of Self-Assembled Structures Made from Inorganic Nanoparticles. *Nat. Nanotechnol.* **2009,** *5*, 15–25.
3. Mao, Z.; Xu, H.; Wang, D. Molecular Mimetic Self-Assembly of Colloidal Particles. *Adv. Funct. Mater.* **2010,** *20*, 1053–1074.
4. Glotzer, S. C. Some Assembly Required. *Science* **2004,** *306*, 419–420.
5. Zhang, Z.; Horsch, M. A.; Lamm, M. H.; Glotzer, S. C. Tethered Nano Building Blocks: Towards a Conceptual Framework for Self-Assembly. *Nano Lett.* **2003,** *3*, 1341–1346.
6. Zhang, Z.; Glotzer, S. C. Self-Assembly of Patchy Particles. *Nano Lett.* **2004,** *4*, 1407–1413.
7. Davis, J. R.; Panagiotopoulos, A. Z. Monte Carol Simulations of Amphiphilic Nanoparticle Self-Assembly. *J. Chem. Phys.* **2008,** *129*, 194706.
8. Iacovella, C. R.; Glotzer, S. C. Complex Crystal Structures Formed by the Self-Assembly of Ditehered Nanospheres. *Nano Lett.* **2009,** *9*, 1206–1211.
9. Whitelam, S.; Bon, S. A. F. Self-Assembly of Amphiphilic Peanut-Shaped Nanoparticles. *J. Chem. Phys.* **2010,** *132*, 074901.
10. Zhang, L.; Eisenberg, A. Multiple Morphologies of "Crew-Cut" Aggregates of Polystyrene-*b*-Poly(acrylic acid) Block Copolymers. *Science* **1995,** *268*, 1728–1731.
11. Blanazs, A.; Armes, S. P.; Ryan, A. J. Self-Assembled Block Copolymer Aggregates: from Micelles to Vesicles and their Biological Applications. *Macromol. Rapid Commun.* **2009,** *30*, 267–277.
12. Zhang, L.; Eisenberg, A. Multiple Morphologies and Characteristics of "Crew-Cut" Micelle-like Aggregates of Polystyrene-*b*-Poly(acrylic acid) Diblock Copolymers in Aqueous Solutions. *J. Am. Chem. Soc.* **1996,** *118*, 3168–3181.

13. Li, Z.; Kesselman, E.; Talmon, Y.; Hillmyer, M. A.; Lodge, T. P. Multicompartment Micelles from ABC Miktoarm Stars in Water. *Science* **2004,** *306*, 98–101.
14. Shen, H.; Eisenberg, A. Morphological Phase Diagram for a Ternary System of Block Copolymer PS_{310}-*b*-PAA_{52}/Dioxane/H_2O. *J. Phys. Chem. B* **1999,** *103*, 9473–9487.
15. Yu, Y.; Zhang, L.; Eisenberg, A. Morphogenic Effect of Solvent on Crew-Cut Aggregates of Amphiphilic Diblock Copolymers. *Macromolecules* **1998,** *31*, 1144–1154.
16. Zubarev, E. R.; Xu, J.; Sayyad, A.; Gibson, J. D. Amphiphilicity-Driven Organization of Nanoparticles into Discrete Assemblies. *J. Am. Chem. Soc.* **2006,** *128*, 15098–15099.
17. Nie, Z.; Fava, D.; Kumacheva, E.; Zou, S.; Walker, G. C.; Rubinstein, M. Self-Assembly of Metal-Polymer Analogues of Amphiphilic Triblock Copolymers. *Nat. Mater.* **2007,** *6*, 609–614.
18. Lattuada, M.; Hatton, T. A. Preparation and Controlled Self-Assembly of Janus Magnetic Nanoparticles. *J. Am. Chem. Soc.* **2007,** *129*, 12878–12889.
19. Nikolic, M. S.; Olsson, C.; Salcher, A.; Kornowski, A.; Rank, A.; Schubert, R.; Fromsdorf, A.; Weller, H.; Forster, S. Micelle and Vesicle Formation of Amphiphilic Nanoparticles. *Angew. Chem., Int. Ed.* **2009,** *48*, 1–4.
20. Zhao, B.; Zhu, L. Mixed Polymer Brush-Grafted Particles: A New Class of Environmentally Responsive Nanostructured Materials. *Macromolecules* **2009,** *42*, 9369–9383.
21. Wang, B.; Li, B.; Dong, B.; Zhao, B.; Li, C. Y. Homo- and Hetero-Particle Clusters Formed by Janus Nanoparticles with Bicompartment Polymer Brushes. *Macromolecules* **2010,** *43*, 9234–9238.
22. Moffitt, M. G.; Zhang, L.; Khougaz, K.; Eisenberg, A. Micellization of Ionic Block Copolymers in Three Dimensions. In *Solvents and Self-Organization of Polymers*; Webber, S. E., Munk, P., Tuzar, Z., Eds.; Kluwer Academic Publishers: Dordrecht, 1996; pp 53−72.
23. Zhang, L.; Yu, K.; Eisenberg, A. Ion-Induced Morphological Changes in "Crew-Cut" Aggregates of Amphiphilic Block Copolymers. *Science* **1996,** *272*, 1777–1779.
24. Zhang, L; Eisenberg, A. Morphogenic Effect of Added Ions on Crew-Cut Aggregates of Polystyrene-*b*-poly(acrylic acid) Block Copolymers in Solutions. *Macromolecules* **1996,** *29*, 8805–8815.
25. Liu, G.; Yan, X.; Li, Z.; Zhou, J.; Duncan, S. End Coupling of Block Copolymer Nanotubes to Nanospheres. *J. Am. Chem. Soc.* **2003,** *125*, 14039–14045.
26. Weaver, J. V. M.; Armes, S. P.; Liu, S. A "Holy Trinity" of Micelles Formed in Aqueous Solution at Ambient Temperature: Unprecedented Self-Assembly Behavior from a Binary Mixture of a Neutral-Cationic Diblock Copolymer and an Anionic Polyelectrolyte. *Macromolecules* **2003,** *36*, 9994–9998.
27. Kubowicz, S.; Baussard, J.-F.; Lutz, J.-F.; Thunemann, A. F.; von Berlepsch, H.; Laschewsky, A. Multicompartment Micelles Formed by Self-Assembly of Linear ABC Triblock Copolymers in Aqueous Medium. *Angew. Chem., Int. Ed.* **2005,** *44*, 5262–5265.
28. Pochan, D. J.; Chen, Z.; Cui, H.; Hales, K.; Qi, K.; Wooley, K. L. Toroidal Triblock Copolymer Assemblies: Advancing the Complexity of Bioinspired Materials. *Science* **2004,** *306*, 94–97.
29. Cui, H.; Chen, Z.; Zhong, S.; Wooley, K. L.; Pochan, D. J. Block Copolymer Assembly *via* Kinetic Control. *Science* **2007,** *317*, 647–650.
30. Hales, K.; Chen, Z.; Wooley, K. L.; Pochan, D. J. Nanoparticles with Tunable Internal Structure from Triblock Copolymers of PAA-*b*-PMA-*b*-PS. *Nano Lett.* **2008,** *8*, 2023–2026.
31. Guo, Y.; Moffitt, M. G. Semiconductor Quantum Dots with Environmentally Responsive Mixed Polystyrene/Poly(methyl methacrylate) Brush Layers. *Macromolecules* **2007,** *40*, 5868–5878.
32. The observed agglomeration of spheres is the result of water evaporation on the TEM grid, and DLS confirms that individual assemblies are well dispersed in the stable aqueous suspensions.
33. Duxin, N.; Liu, F.; Vali, H.; Eisenberg, A. CdS QDs in Morphologically Tunable Triblock Copolymer Aggregates. *J. Am. Chem. Soc.* **2005,** *127*, 10063–10069.
34. The fully stretched dimension of a 296-unit PS chain is 74 nm. Since some PS blocks must span the mean radial core distance of 70 nm, it appears that PS chains in the supermicelles are up to 95% fully stretched.
35. Jain, S.; Bates, F. S. On the Origins of Morphological Complexity in Block Copolymer Surfactants. *Science* **2003,** *300*, 460–464.
36. Discher, B. M.; Won, Y.-Y.; Ege, D. S.; Lee, J. C.-M.; Bates, F. S.; Discher, D. E.; Hammer, D. A. Polymersomes: Tough Vesicles Made from Diblock Copolymers. *Science* **1999,** *284*, 1143–1146.
37. Discher, D. E.; Eisenberg, A. Polymer Vesicles. *Science* **2002,** *297*, 967–973.
38. Hautekeer, J.-P.; Varshney, S. K.; Fayt, R.; Jacobs, C.; Jerome, R.; Teyssie, P. Anionic Polymerization of Acrylic Monomers. 5. Synthesis, Characterization, and Modification of Polystyrene−Poly(*tert*-butyl acrylate) Di- and Triblock Copolymers. *Macromolecules* **1990,** *23*, 3893–3898.
39. Zhong, X. F.; Varshney, S. K.; Eisenberg, A. Critical Micelle Lengths for Ionic Blocks in Solutions of Polystyrene-*b*-Poly(sodium acrylate) Ionomers. *Macromolecules* **1992,** *25*, 7160–7167.
40. Kang, Y.; Taton, T. Micelle-Encapsulated Carbon Nanotubes: A Route to Nanotube Composites. *J. Am. Chem. Soc.* **2003,** *125*, 5650–5651.
41. Kang, Y.; Taton, T. Core/Shell Gold Nanoparticles by Self-Assembly and Crosslinking of Micellar, Block-Copolymer Shells. *Angew. Chem., Int. Ed.* **2005,** *44*, 409–412.
42. Kang, Y.; Taton, T. Controlling Shell Thickness in Core-Shell Gold Nanoparticles *via* Surface-Templated Adsorption of Block Copolymer Surfactants. *Macromolecules* **2005,** *38*, 6115–6121.